University of Wollongong
Research Online

Faculty of Engineering - Papers (Archive)

Faculty of Engineering and Information Sciences

2011

Highly porous metal oxide polycrystalline nanowire films with superior performance in gas sensors

Jun Liu
junliu@uow.edu.au

Zaiping Guo
University of Wollongong, zguo@uow.edu.au

Kaixing Zhu
Chinese Academy of Sciences, Beijing

Wenjun Wang
Institute of Physics Chinese Academy of Sciences

Chaofeng Zhang
University of Wollongong, cz583@uow.edu.au

See next page for additional authors

Publication Details

Liu, J., Guo, Z., Zhu, K., Wang, W., Zhang, C. & Chen, X. (2011). Highly porous metal oxide polycrystalline nanowire films with superior performance in gas sensors. Journal of Materials Chemistry, 21 (30), 11412-11417.

Research Online is the open access institutional repository for the University of Wollongong. For further information contact the UOW Library: research-pubs@uow.edu.au

Authors
Jun Liu, Zaiping Guo, Kaixing Zhu, Wenjun Wang, Chaofeng Zhang, and Xiaolong Chen

This journal article is available at Research Online: http://ro.uow.edu.au/engpapers/1415

View Online / Journal Homepage / Table of Contents for this issue
Dynamic Article Links

Journal of Materials Chemistry

Cite this: *J. Mater. Chem.*, 2011, **21**, 11412

www.rsc.org/materials

PAPER

Highly porous metal oxide polycrystalline nanowire films with superior performance in gas sensors†

Jun Liu,[a] Zaiping Guo,*[a] Kaixing Zhu,[b] Wenjun Wang,[b] Chaofeng Zhang[a] and Xiaolong Chen*[b]

Received 4th February 2011, Accepted 19th May 2011
DOI: 10.1039/c1jm10537j

Downloaded by University of Wollongong on 03 April 2012
Published on 28 June 2011 on http://pubs.rsc.org | doi:10.1039/C1JM10537J

In this work, we report for the first time a simple two-step route to fabricate a novel porous metal oxide film composed of polycrystalline nanowires with ultra-small nanoparticles, good interconnectivity between nanoparticles, and a high density of ultra-fine nanopores. The as-prepared metal oxide films combine the advantages of small crystal size, high surface-to-volume ratio, and one-dimensional-nanowire-induced unique charge transport paths (with correspondingly high interconnectivity). Taking In_2O_3 as an example, porous In_2O_3 films, composed of polycrystalline In_2O_3 nanowires with ultra-small nanocrystals (less than 10 nm) and a high density of ultra-fine nanopores (1.6–3.1 nm), have shown very high sensitivity and good reproducibility towards ethanol gas, which are 10–20 times higher than for In_2O_3 octahedra and commercial SnO_2 thick films. The response/recovery speeds of the as-prepared porous In_2O_3 films are also 5–6 times higher than for In_2O_3 octahedra, SnO_2 nanobelts, and commercial SnO_2 thick films. We believe that such metal oxide flexible films made from highly porous nanowires will replace their traditional thick film counterparts, not only in gas sensors but also in other functional devices, such as batteries, supercapacitors, solar cells, *etc.*

Introduction

Almost half a century ago, it was realized that semiconducting metal oxides had great potential as gas-sensing materials,[1] owing to the fact that the chemical interaction of gas molecules with the semiconductor surface leads to changes in the electrical conductivity. Such "chemiresistors" can be manufactured as portable devices that can be operated at elevated temperature by battery power and used in a large variety of applications, such as fire detectors, leakage detectors, controllers of ventilation in cars and airplanes, and alarm devices warning that concentrations of hazardous gases have exceeded preset thresholds in workplaces. They can even be used for the detection of smells generated from food or household products and for analysis of complex environmental mixtures.[2–5] The sensing material is usually deposited as a thick solid film or layer on a substrate with electrodes, as shown in Scheme 1(a). Such ethanol sensors based on SnO_2 thick films have been commercialized for years. However, the gas

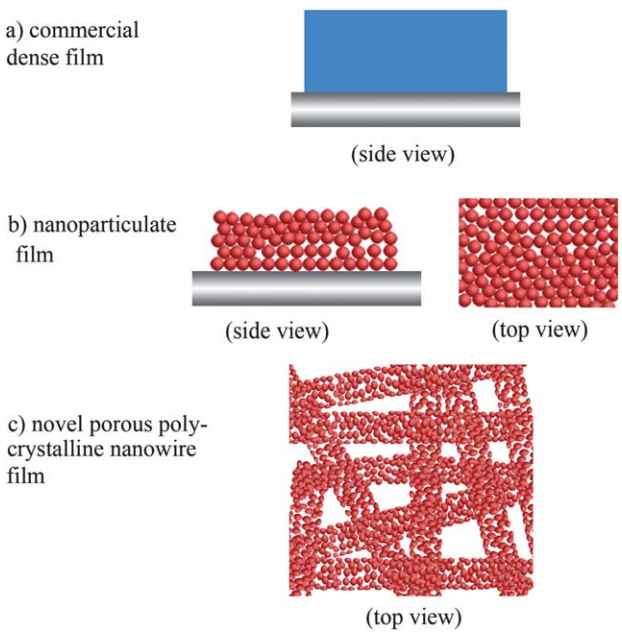

Scheme 1 Schematic diagrams of gas sensor films: (a) commercial dense film, which suffers from large crystal sizes and low surface area; (b) nanoparticulate film, in which it is difficult to achieve both large surface area (realized by low grain interconnectivity) and high stability/electronic conductance (resulting from high grain interconnectivity); (c) novel porous polycrystalline nanowire film with small nanocrystal sizes, ultra-high surface area, and one-dimensional (1D)-nanowire-induced unique charge transport paths (with correspondingly high interconnectivity).

[a]*Institute for Superconducting and Electronic Materials, University of Wollongong, NSW, 2522, Australia. E-mail: zguo@uow.edu.au; Fax: +61 2 4221 5731; Tel: +61 2 4221 5225*
[b]*Beijing National Laboratory for Condensed Matter Physics, Institute of Physics, Chinese Academy of Sciences, Beijing, 100190, China. E-mail: chenx29@aphy.iphy.ac.cn; Fax: +86-010-82649646; Tel: +86-010-82649036*

† Electronic supplementary information (ESI) available: Photograph of synthesized gram-scale InN nanowires, SEM images of InN nanowires, experimental details for synthesis of In_2O_3 octahedra and SnO_2 nanobelts, together with XRD patterns and SEM images. See DOI: 10.1039/c1jm10537j

This journal is © The Royal Society of Chemistry 2011

Downloaded by University of Wollongong on 03 April 2012
Published on 28 June 2011 on http://pubs.rsc.org | doi:10.1039/C1JM10537J

sensitivities of these traditional thick, dense films have been intrinsically restricted by their large crystal sizes and low surface areas, and applications of these traditional thick films are also limited by their lack of flexibility. Although atomic layer deposition (ALD)[5,6] and molecular beam epitaxy (MBE)[7] have been recently used to produce dense films with thicknesses within the Debye length, δ (such as $\delta \approx 3$ nm for SnO_2 at 250 °C),[8] from the viewpoint of high gas sensitivity, these dense films still suffer from high sensor resistance and poor mechanical stability.

In 1991, Yamazoe demonstrated that reduction in the crystal size of metal oxides would significantly increase their sensor performance.[9] This is because the grains of nanomaterials are almost depleted of carriers, and changes in the surface oxygen concentration significantly affect the whole semiconductor, resulting in high sensitivity.[10] Therefore, in the past two decades, many wet and dry methods, such as sol–gel synthesis,[11,12] chemical or physical vapor deposition,[13,14] spray pyrolysis,[15] pulsed laser deposition,[16] and sputtering,[17] have been developed to synthesize metal oxide nanoparticles and assemble them into nanoparticulate films, as shown in Scheme 1(b). The main advantage of nanoparticulate films in comparison to dense films is that it is not necessary to decrease the film thickness down to the Debye length of the oxide to reach high sensitivity. However, to date, it is still difficult to achieve controlled production of nanoparticulate films with both large surface areas (realized by low grain agglomeration) and high stability/electronic conductance (resulting from high grain interconnectivity). Therefore, new methods and technologies for fabrication of small nanocrystals with both high grain interconnectivity and large surface areas must be developed.

Synthesis of porous metal oxide films is also a good method to enhance gas sensitivity due to their high surface areas. Most syntheses of porous metal oxide films reported so far have focused on template-assisted methods.[18,19] Recently, there have been a few reports on the preparation of porous metal oxide powders by chemical conversion methods, such as chemical conversion from $CdCO_3$ to CdO,[20] from CuS to CuO,[21] and from cobalt hydroxide to Co_3O_4.[22a] Although these methods can produce porous metal oxide films or powders, it is still hard to separately control the film thickness, and the grain and crystal sizes. These strategies also often produce porous materials with pore sizes in the range of several tens of nanometres or up to hundreds of nanometres, due to the limitations of template sizes or large volume loss in the chemical conversion.

In this paper, we report a chemical conversion strategy to synthesize and self-assemble ultra-small metal oxide nanocrystals into polycrystalline nanowires with a high density of ultra-fine nanopores. The porous polycrystalline nanowires are then matted into a porous nanowire film (as shown in Scheme 1(c)) by a simple filtration method. Such a two-step route presents a feasible way to separately control the thickness of the porous film and the crystal size. The first step is based on a chemical conversion from metal nitride nanowires to porous metal oxide polycrystalline nanowires. Compared to previous work,[20–22a] our porous metal oxides produced by a chemical conversion from metal nitrides feature ultra-fine nanopores. Herein, taking In_2O_3[22b–d] as an example, porous In_2O_3 films, composed of polycrystalline In_2O_3 nanowires with ultra-small nanocrystals (less than 10 nm) and a high density of ultra-fine nanopores (1.6–3.1 nm), have been successfully synthesized and show very high sensitivity towards ethanol gas, 10–20 times higher than for commercial SnO_2 thick films. The response/recovery speeds of the as-prepared porous In_2O_3 films are also 5–6 times higher than for SnO_2 nanobelts and commercial SnO_2 thick films. At the same time, these tunable, scalable, and reproducible porous metal oxide films can also be readily integrated into flexible gas sensor devices. We believe that such deliberately designed thin, flexible metal oxide films made from highly porous nanowires will replace their traditional thick film counterparts, not only in gas sensors but also in other applications, such as catalysts, batteries, supercapacitors, solar cells, *etc.*, due to their much smaller crystal size, higher surface-to-volume ratio, and unique charge transport paths.

Experimental

The synthesis of the novel In_2O_3 films made from porous In_2O_3 nanowires consists of a two-step route. Synthesis of porous In_2O_3 nanowires is based on a chemical conversion: In_2O_3 powder (3 g, 99.99%) is put into an ethanol solution for ultrasonic treatment, and then, this solution containing In_2O_3 powder is evenly coated on the walls of a quartz boat (23 cm × 3 cm × 1.5 cm) by slowly drying it. The quartz boat is placed in the central heating zone of the quartz tube in a tube furnace. The quartz tube is pumped and then filled with pure ammonia (NH_3). After repeating the operation three times, the quartz tube is heated to 660 °C in half an hour under a pure ammonia flow of 400 standard cubic centimetres per minute (sccm) and normal pressure. After the quartz tube has been kept at this temperature for 24 hours, it is naturally cooled. Then, the large amount of wool-like product (InN nanowires) in the quartz boat is heated to 600 °C in 180 minutes under air atmosphere. After it is annealed for 2 hours at this temperature, it is naturally cooled. The synthesis of porous In_2O_3 nanowire film is based on a simple filtration method: the annealed products (porous In_2O_3 nanowires) are collected and put into 50 ml of Milli-Q water, followed by stirring for several minutes. A porous anodic aluminium oxide (AAO) membrane with a pore size of 220 nm acts as a filter paper. Passing the prepared In_2O_3 suspension through the AAO filter in a filtration cell under a positive nitrogen gas pressure of 400 kPa produces a flexible mat of entangled porous In_2O_3 nanowires, known as a "bucky paper" from its carbon nanowire equivalent. The In_2O_3 nanowire mat is peeled off the AAO filter after letting it dry overnight in a vacuum oven. The thickness of the In_2O_3 nanowire paper can be easily tuned by changing the amount of porous In_2O_3 nanowires.

Phase identifications were performed on an X-ray diffractometer (Philips X'PERT MPD) with Cu Kα radiation (λ = 1.5406 Å), operated at 40 kV and 40 mA. The morphologies and microstructures of the product were characterized using scanning electron microscopy (Hitachi, S-4200) and transmission electron microscopy (Philip, CM-2000FEG). The Brunauer–Emmett–Teller (BET) surface area measurement and pore analysis were carried out by nitrogen adsorption with the use of a Micromeritics ASAP 2020 V3.00H surface area analyser. The measurement was carried out at liquid nitrogen temperature after degassing the powder sample at 250 °C. The thermogravimetric/differential thermal analysis (TGA-DTA) experiment was

Downloaded by University of Wollongong on 03 April 2012
Published on 28 June 2011 on http://pubs.rsc.org | doi:10.1039/C1JM10537J

performed on an SDT Q600 (V20.9 Build 20) instrument. InN nanowires were put into an alumina crucible and heated in air at 10 °C min^{-1} from room temperature to a final temperature of 800 °C.

The gas-sensing tests were performed in a WS-60A measurement system (Zhengzhou Winsen Electronics Technology, China). In a typical test, a gas sensor was fabricated by attaching a porous In_2O_3 nanowire film onto a ceramic disk that had been previously mounted with gold electrodes and platinum conducting wires (ESI†, Fig. S1). A resistor wire was inserted under the disk as a heater to provide working temperatures from 200 to 500 °C by varying the heating current. The ethanol was injected onto a metal-plate heater in the test chamber and evaporated completely by heating. The gas-sensing capability of the sensor was defined as the ratio R_{gas}/R_{air}, where R_{gas} and R_{air} are the electrical resistance of the sensor in test gas and in air at the working temperature of about 260 °C, respectively.

Results and discussion

Fig. 1 shows X-ray diffraction (XRD) patterns of the products, as-obtained by nitriding In_2O_3 powders (a) and after further annealing for 2 hours in air (b). The XRD pattern of the products in the first step can be well indexed to a hexagonal cell with $a = b = 3.538$ Å and $c = 5.703$ Å, in good agreement with the standard data (ICDD-PDF 50-1239), confirming that the product obtained by nitriding In_2O_3 is InN with a hexagonal structure. The XRD pattern of the product annealed for 2 hours in air can be well indexed to a cubic cell with $a = b = c = 10.140$ Å, in good agreement with the standard data (ICDD-PDF 65-3170), confirming that this product is pure In_2O_3 with a cubic structure. According to the full width at half maximum (FWHM) of each peak in the XRD patterns, it can be deduced from the Scherrer formula that the crystal sizes of In_2O_3 (5–10 nm) are much smaller than those of InN (about 40 nm).

The photograph in Fig. S2(a)† shows the gram-scale synthesis of rufous wool-like InN obtained in the first step, which is sufficient to fill up a quartz boat (23 cm × 3 cm × 1.5 cm). The scanning electron microscope (SEM) images in Fig. S2(b) and (c)† show that the synthesized wool-like InN consists of a large amount of nanowires with a uniform diameter of around 40 nm. The transmission electron microscope (TEM) image in Fig. S2(d)† and the corresponding high resolution TEM (HRTEM) image in Fig. S2(e)† indicate that these InN nanowires are single crystals with excellent crystallinity and grow along the [001] direction. The photograph in Fig. 2(a) shows the gram-scale synthesis of a yellowish wool-like product in the second step, also sufficient to fill up a quartz boat (23 cm × 3 cm × 1.5 cm). The SEM image in Fig. 2(b) shows that the synthesized wool-like product consists of a large amount of In_2O_3 nanowires with a uniform diameter of about 40 nm. The TEM images in Fig. 2(c) and S3(a)† indicate that the as-synthesized In_2O_3 nanowire is polycrystalline and has a preferred orientation along the [222] direction, which is demonstrated in the corresponding selected area electron diffraction (SAED) pattern (inset in Fig. S3(a)†). Moreover, it is interesting to note that these In_2O_3 nanowires all have a high density of nanopores, as shown in Fig. S3(b) and (c)†.

Nitriding In_2O_3 in an NH_3 flux to synthesize InN micro- and nanostructures has been reported by some groups.[23–25] Compared to these previous works, we have scaled up the reaction to demonstrate its potential for gram-scale synthesis of long InN nanowires with a uniform diameter of about 40 nm by *in situ* nitriding of In_2O_3 commercial micropowders. Because no catalyst is involved, the vapor–solid (VS) mechanism should account for the formation of the InN nanowires. The formation of porous In_2O_3 nanowires with a high density of ultra-fine nanopores is illustrated in Scheme 2. Thermodynamically, the oxidation reaction ($2InN + (3/2)O_2 \rightarrow In_2O_3 + N_2$) is expected to occur readily when InN is exposed to an oxygen-containing atmosphere, due to the large difference in the heat of formation at room temperature between InN (−4.2 kcal mol^{-1}) and In_2O_3 (−221.27 kcal mol^{-1}),[26] as shown in Scheme 2(A). The DTA-TGA curves obtained for the InN precursor under air atmosphere are shown in Fig. S4†. At the beginning of the thermal oxidation of InN, a thin In_2O_3 shell is formed on the surface of these nanowires. This thin layer acts as an interface and prevents the inner InN from coming into direct contact with the outer atmospheric oxygen. However, the interface consists of an intermediate shell with many vacancies. This kind of shell

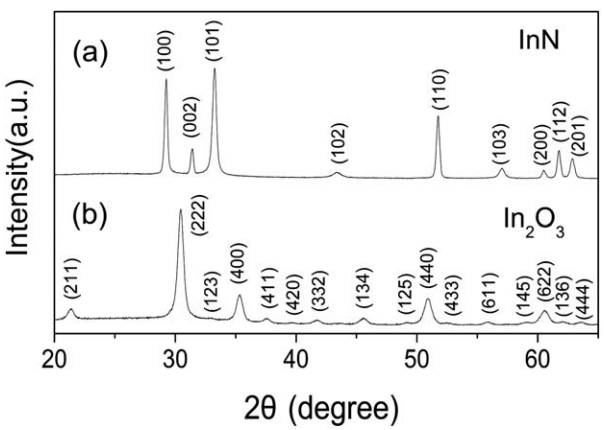

Fig. 1 XRD patterns of the product in the first step (a) and the product after annealing for 2 hours at 600 °C in air (b).

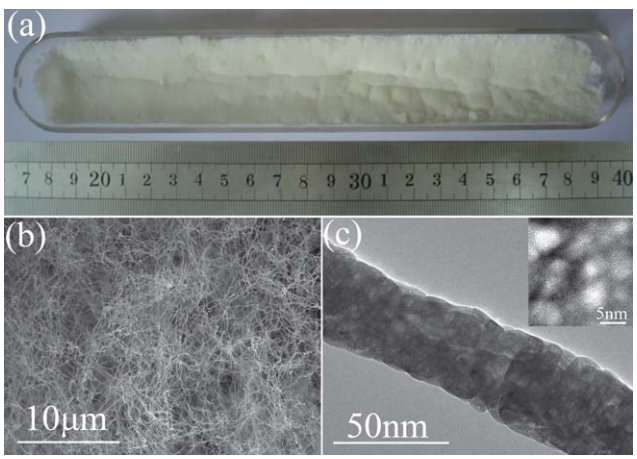

Fig. 2 (a) Photograph of gram-scale synthesized porous In_2O_3 nanowires; (b) SEM image of the as-synthesized porous In_2O_3 nanowires created by a chemical conversion from InN nanowires; (c) TEM image and HRTEM image (inset) of an as-synthesized porous In_2O_3 nanowire, showing its high density of ultra-fine nanopores.

 This journal is © The Royal Society of Chemistry 2011

Downloaded by University of Wollongong on 03 April 2012
Published on 28 June 2011 on http://pubs.rsc.org | doi:10.1039/C1JM10537J

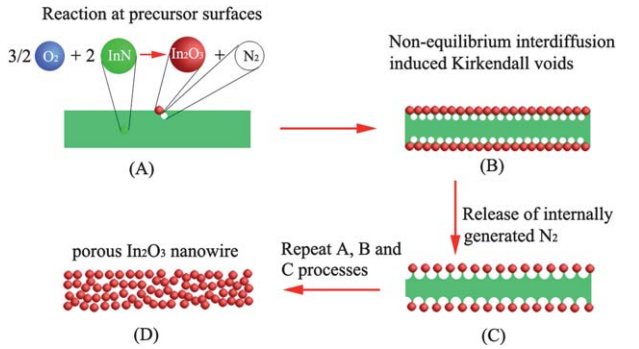

Scheme 2 Schematic diagram of the procedure used to fabricate porous In_2O_3 hollow architectures: (A) uniform InN is used as the starting precursor; (B) formation of In_2O_3 shell on the surface of InN in the thermal oxidation process, with Kirkendall voids formed at the interface which results from the non-equilibrium interdiffusion; (C) formation of porous In_2O_3 shell on the surface of InN, which results from volume loss and release of internally generated N_2; (D) A, B, and C processes are repeated to chemically convert InN nanowires into highly porous In_2O_3 nanowires.

structure allows the outward diffusion of the inner nitrogen atoms and vacancies, and the inward diffusion of oxygen. Since the outward diffusion rate of the inner nitrogen is larger than the inward diffusion rate of atmospheric oxygen during the oxidation reactions, small voids are thus generated in the interface of InN/In_2O_3 (as shown in Scheme 2(B)). Such non-equilibrium interdiffusion is known as the "Kirkendall Effect", which has been introduced into nanomaterial synthesis (such as in the synthesis of nanocrystals,[27] peashell-like nanostructures,[28] and nanotubes[29]) and has been well explained by Fan *et al.*[30] The newly formed In_2O_3 shell forms a coating on the InN nanowires, which can effectively block the release of internally generated gas. More gas accumulates gradually in the interior of the structure until the pressure is increased to the point where the structure is broken to form a small pore, and finally, a porous shell is formed, as shown in Scheme 2(C). Once the porous shell is formed, the atmospheric oxygen can directly react with the inner InN, by a process which is similar to the thermal oxidation of InN nanowires in the very beginning. Then, the In_2O_3 shell can be formed again, and small voids will be generated in the interface. Such a process will be repeated until the whole InN nanowire has been transformed into a porous In_2O_3 polycrystalline nanowire, as shown in Scheme 2(D). Therefore, the formation of porous In_2O_3 nanowires is based on non-equilibrium interdiffusion (the Kirkendall effect), volume loss, and gas release. Moreover, it is interesting that the as-synthesized porous In_2O_3 nanowires produced by chemical conversion from InN have ultra-fine nanopores (1.6–3.1 nm) compared to those previously reported. For example, in reducing Mn_3O_4 to MnO, the pore sizes are about 50 nm;[31] in oxidising CuS to synthesize CuO, the pore sizes are about 100 nm;[21] in annealing $Co(OH)_2$ to synthesize Co_3O_4, the pore sizes are about 50 nm;[22a] and in annealing $CdCO_3$ to synthesize CdO, the pore sizes are about 50 nm.[20] This is possibly because the diameter of the as-synthesized InN nanowires is less than 50 nm, and such small InN nanowires as starting reactants will enhance N_2 gas release, so as to avoid large pore formation. However, in those microscale materials previously reported as starting reactants, gas diffusion over long distances is required.

In order to fabricate a sensor film with small crystal size, high surface area, and high grain interconnectivity, these porous and polycrystalline In_2O_3 nanowires are filtered in a filtration cell under a positive nitrogen gas pressure of 400 kPa to produce a tight and flexible mat of entangled porous In_2O_3 nanowires, known as a "bucky paper". Fig. 3(a) presents a photograph of the flexible film. The flexible film with entangled porous In_2O_3 nanowires is also shown in an enlarged SEM image (Fig. 3(b)). The specific surface area and pore size distribution of the porous In_2O_3 nanowire film were measured by BET N_2 adsorption after degassing at 250 °C for 12 h, as shown in Fig. 4. It can be seen that the specific surface area is as high as 185.38 $m^2\ g^{-1}$. The pore size distribution in the film ranged from 1.6 nm to 3.1 nm, and from 10 nm to 250 nm, with a maximum at 2.2 nm. The pores ranging from 1.6 nm to 3.1 nm correspond to the small pores formed in In_2O_3 nanowires, but the pores ranging from 10 nm to 250 nm correspond to the holes between the different In_2O_3 nanowires.

Such a novel flexible film can be readily cut into a small sheet and simply attached onto an Al_2O_3 substrate with electrodes to make a sensor device (Fig. S1†). Fig. 5 shows the gas sensitivity and response/recovery speeds of the as-prepared porous In_2O_3 nanowire films compared to In_2O_3 octahedra, commercial SnO_2 thick, dense films, and SnO_2 nanobelts towards different concentrations of ethanol gas at 260 °C. (SnO_2 is the most widely used gas sensing material.) The experimental details for large-scale synthesis of In_2O_3 octahedra and SnO_2 nanobelts, along with the XRD patterns and SEM images of these In_2O_3 octahedra and as-synthesized SnO_2 nanobelts, are shown in the ESI†. It can be seen that the sensors using porous In_2O_3 nanowire films show stable response and recovery behavior. The gas responses of porous In_2O_3 nanowire films (R_{air}/R_{gas}, R_{air}: resistance in air, R_{gas}: resistance in gas) to 2, 20, 50, and 100 ppm C_2H_5OH are up to 2.06, 14.88, 38.6, and 62.6, respectively, which are 10–20 times higher than for In_2O_3 octahedra and commercial SnO_2 thick films. The times to reach 90% variation in resistance upon exposure to C_2H_5OH and air are defined as the 90% response time (τ_{res}) and the 90% recovery time (τ_{recov}), respectively. The τ_{res} values of the porous In_2O_3 nanowire films upon exposure to 2, 20, 50, and 100 ppm C_2H_5OH are 6, 4, 3, and 5 s, respectively, whereas the τ_{res} values of In_2O_3 octahedra on average are 30 s, the τ_{res} values of SnO_2 nanobelts on average are 23 s, and the τ_{res} values of the commercial SnO_2 thick films are 20 s. The τ_{recov}

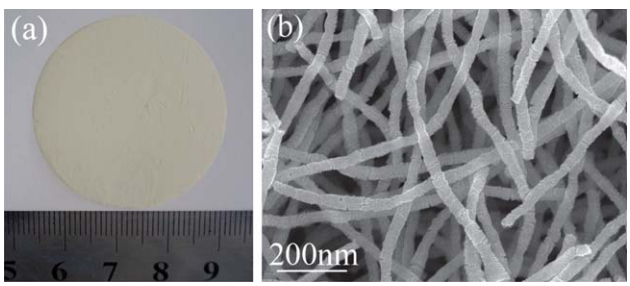

Fig. 3 Photograph (a) and enlarged SEM image (b) of a porous In_2O_3 nanowire film.

Downloaded by University of Wollongong on 03 April 2012
Published on 28 June 2011 on http://pubs.rsc.org | doi:10.1039/C1JM10537J

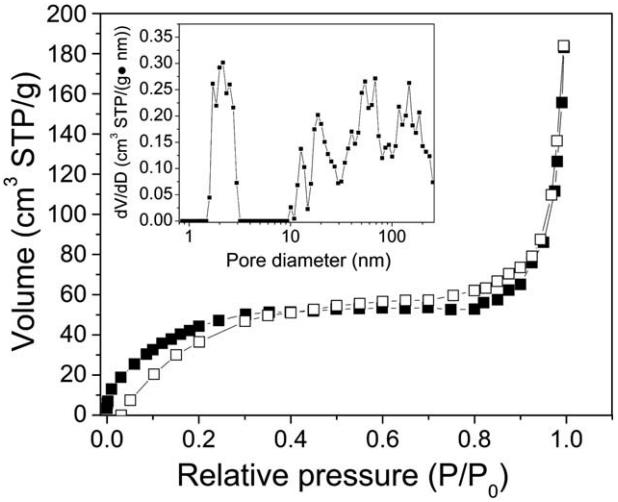

Fig. 4 N_2 adsorption–desorption isotherms and pore size distribution (inset) of the porous In_2O_3 nanowire film.

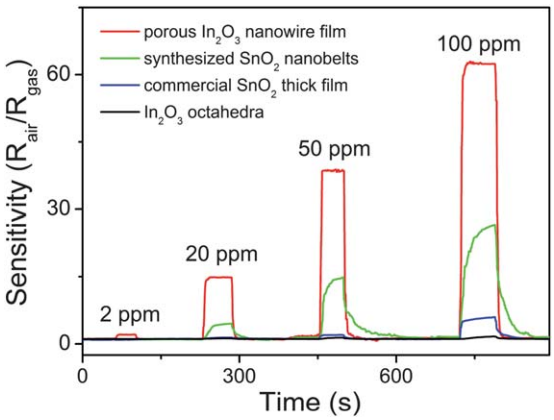

Fig. 5 The gas sensitivities and response times of porous In_2O_3 nanowire films, In_2O_3 octahedra, SnO_2 nanobelts, and commercial SnO_2 thick, dense films towards different concentrations of ethanol gas at 260 °C.

values of the porous In_2O_3 nanowire films during recovery after exposure to 2, 20, 50, and 100 ppm C_2H_5OH are 7, 5, 4, and 7 s, respectively (as is shown in Table S1†), whereas the τ_{recov} values of SnO_2 nanobelts on average are 41 s, the τ_{recov} values of SnO_2 nanobelts on average are 37 s, and the τ_{recov} values of the commercial SnO_2 thick films are 30 s. Therefore, the response/recovery speeds of porous In_2O_3 nanowire films are 5–6 times higher than for In_2O_3 octahedra, the SnO_2 nanobelts, or the commercial SnO_2 thick films. The long-term stability test results on porous In_2O_3 nanowire film sensors exposed to 50 ppm ethanol gas at 260 °C are shown in Fig. S10†, and it can be seen that the gas sensitivity of the porous In_2O_3 nanowire film sensors can be maintained for at least 120 days. Fig. S11† shows the variation of sensitivity of porous In_2O_3 nanowire film sensors with the thickness for four values of concentrations of ethanol vapor. As is evident from the figure, the sensitivity of the sensors increases with increasing vapor concentration and decreasing thickness of the gas sensor film. Fig. S12† shows the stability of the response of porous In_2O_3 nanowire film sensors with different thicknesses to 50 ppm ethanol gas at 260 °C.

As is well known, when a metal oxide gas sensor is exposed to air, oxygen species can be adsorbed on the surface of the sensor, and then are ionized into O^- or O^{2-} by capturing free electrons from the conductance band of the metal oxide. Therefore, as a pronounced n-type semiconductor, In_2O_3 will show a decrease in conductivity in air due to the decreased concentration of free electrons. This process can be depicted as follows:[32]

$$O_2\ (gas) \leftrightarrow O_2\ (adsorption) \quad (1)$$

$$O_2\ (gas) + e \leftrightarrow O_2^-\ (adsorption) \quad (2)$$

$$O_2^-\ (adsorption) + e \leftrightarrow 2O^-\ (adsorption) \quad (3)$$

$$O_2^-\ (adsorption) + e \leftrightarrow O^{2-}\ (adsorption) \quad (4)$$

When the sensor is exposed to a reducing gas such as ethanol gas, the reducing gas may react with the adsorbed and ionized oxygen molecules and release the trapped electrons back into the In_2O_3 semiconductor, thereby increasing the conductivity of In_2O_3. This can simply be described as follows:[32,33]

$$C_2H_5OH + 6O^-\ (adsorption) \rightarrow 2CO_2 + 3H_2O + 6e^- \quad (5)$$

$$C_2H_5OH + 6O^{2-}\ (adsorption) \rightarrow 2CO_2 + 3H_2O + 12e^- \quad (6)$$

Therefore, the oxygen adsorption in the first step is very important for the performance of the sensor. The excellent gas sensor properties of the as-prepared In_2O_3 flexible films may be related to the following factors: (1) crystal sizes are very small, which induces high chemical reactivity and favors the adsorption and ionization of oxygen molecules on their surfaces. In addition, such small nanosized grains of In_2O_3 (with a size approximately twice the Debye length) cause whole grains to be depleted of carriers and exhibit much poorer conductivity than SnO_2 nanobelts and commercial SnO_2 thick films in ambient air. (2) Surface-to-volume ratios are ultra-high, so that gas sensors containing such films can adsorb a much greater amount of oxygen molecules than the gas sensors based on SnO_2 nanobelts and commercial SnO_2 thick films. These two factors have also been reported in many papers.[34–39] (3) The final factor is the one-dimensional (1D) nanowire shape, which gives the small constituent nanocrystals higher grain interconnectivity compared to loosely packed nanoparticles with tiny interparticle contact areas. The τ_{res} values of the In_2O_3 flexible films are significantly shorter (3–6 s) compared to what has been reported in the literature,[40] which reveals the fast gas diffusion in the sensor. Such fast gas diffusion is the result of the highly porous nature of the In_2O_3 nanowire film with its ultra-high surface-to-volume ratio, which allows faster gas diffusion into and out of the sensing layers. Moreover, due to the high working temperature (260 °C), the oxygen diffusion at the surface of the porous In_2O_3 nanowire films will be much faster than at room temperature. The recovery reaction includes the following serial reactions: the diffusion of oxygen onto the sensing surface, the adsorption of oxygen, and the dissociation and ionization of oxygen.[40] With both much smaller crystal sizes and ultra-high surface-to-volume ratios, the In_2O_3 flexible films exhibit high chemical reactivities and can more easily adsorb and ionize oxygen at a high working temperature (260 °C). The superior

 This journal is © The Royal Society of Chemistry 2011

recovery time is attributable to this promotion of surface reactions involving adsorption, dissociation, and ionization of oxygen.

Conclusion

In conclusion, we have reported for the first time a novel porous metal oxide film consisting of polycrystalline nanowires with ultra-small nanocrystals and a high density of ultra-fine nanopores, which was synthesized by a chemical conversion technique followed by filtration. The two-step method provides a feasible way to separately control the thickness of the porous film and the crystal size. Compared to previous reports, the as-synthesized metal oxide nanowires feature ultra-fine nanopores. Taking In_2O_3 as an example, porous and flexible In_2O_3 films, made of In_2O_3 polycrystalline nanowires with ultra-small nanocrystals (less than 10 nm) and a high density of ultra-fine nanopores (1.6–3.1 nm), have been successfully synthesized and show significantly higher sensitivities, as well as good reproducibility and faster response/recovery speeds towards ethanol gas compared to both commercial SnO_2 thick films and SnO_2 nanobelts because of their much smaller crystal sizes, ultra-high surface-to-volume ratios, nanoporous structure, and 1D nanowire structure, which induces unique charge transport paths. We believe that such functionally designed metal oxide flexible films will replace their traditional thick film counterparts, not only in gas sensors but also possibly in other functional devices.

Acknowledgements

This work is partly supported by the Australian Research Council through a Discovery Project (DP1094261), the National Basic Research Program of China (973 Program) grant No. 2007CB936300, the National High Technology Research and Development Program of China (863 Program) grant No. 2006AA03A107, and the National Natural Science Foundation of China (grant No. 50702073). We thank Dr Tania Silver for the English editing of this paper.

Notes and references

1 T. Seiyama, A. Kato, K. Fujiishi and M. Nagatani, *Anal. Chem.*, 1962, **34**, 1502–1503.
2 J. Du, D. Liang, H. Tang and X. Gao, *Nano Lett.*, 2009, **9**, 4348–4351.
3 N. Du, H. Zhang, B. D. Chen, X. Y. Ma, Z. H. Liu, J. B. Wu and D. R. Yang, *Adv. Mater.*, 2007, **19**, 1641–1645.
4 X. G. Han, M. S. Jin, S. F. Xie, Q. Kuang, Z. Y. Jiang, Y. Q. Jiang, Z. X. Xie and L. S. Zhang, *Angew. Chem., Int. Ed.*, 2009, **48**, 9180–9183.
5 A. Rosental, A. Tarre, A. Gerst, T. Uustare and V. Sammelselg, *Sens. Actuators, B*, 2001, **77**, 297.
6 A. Rosental, A. Tarre, A. Gerst, J. Sundqvist, A. Hrsta, A. Aidla, J. Aarik, V. Sammelselg and T. Uustare, *Sens. Actuators, B*, 2003, **93**, 552.
7 M. Kroneld, S. Novikov, S. Saukko, P. Kuivalainen, P. Kostamo and V. Lantto, *Sens. Actuators, B*, 2006, **118**, 110.
8 H. Ogawa, M. Nishikawa and A. Abe, *J. Appl. Phys.*, 1982, **53**, 4448.
9 N. Yamazoe, New approaches for improving semiconductor gas sensors, *Sens. Actuators, B*, 1991, **5**, 7–19.
10 A. Rothschild and Y. Komem, *J. Appl. Phys.*, 2004, **95**, 6374.
11 E. R. Leite, I. T. Weber, E. Longo and J. A. Varela, *Adv. Mater.*, 2000, **12**, 956–968.
12 N. Pinna, G. Neri, M. Antonietti and M. Niederberger, *Angew. Chem., Int. Ed.*, 2004, **116**, 4445–4449.
13 Y. Liu, E. Koep and M. L. Liu, *Chem. Mater.*, 2005, **17**, 3997.
14 S. Peulon and D. Lincot, *Adv. Mater.*, 1996, **8**, 166.
15 A. Tricoli, M. Graf and S. E. Pratsinis, *Adv. Funct. Mater.*, 2008, **18**, 1969.
16 R. Khandelwal, A. P. Singh, A. Kapoor, S. Grigorescu, P. Miglietta, N. E. Stankova and A. Perrone, *Opt. Laser Technol.*, 2009, **41**, 89.
17 Y. H. Choi and S. H. Hong, *Sens. Actuators, B*, 2007, **125**, 504.
18 R. H. A. Ras, M. Kemell, J. D. Wit, M. Ritala, G. T. Brinke, M. Leskelä and O. Ikkala, *Adv. Mater.*, 2007, **19**, 102.
19 M. G. Han and S. H. Foulger, *Chem. Commun.*, 2004, 2154–2155.
20 H. D. Yu, D. S. Wang and M. Y. Han, *J. Am. Chem. Soc.*, 2007, **129**, 2333–2337.
21 J. Liu and D. F. Xue, *Adv. Mater.*, 2008, **20**, 1–6.
22 (*a*) L. Tian, H. L. Zou, J. X. Fu, X. F. Yang, Y. Wang, H. L. Guo, X. H. Fu, C. L. Liang, M. M. Wu, P. K. Shen and Q. M. Gao, *Adv. Funct. Mater.*, 2010, **20**, 617–623; (*b*) P. C. Xu, Z. X. Cheng, Q. Y. Pan, J. Q. Xu, Q. Xiang, W. J. Yu and Y. L. Chu, *Sens. Actuators, B*, 2008, **130**, 802–808; (*c*) J. Y. Lao, J. Y. Huang, D. Z. Wang and Z. F. Ren, *Adv. Mater.*, 2004, **16**, 65–69; (*d*) Lin Xu, B. Dong, Y. Wang, X. Bai, Q. Liu and H. W. Song, *Sens. Actuators, B*, 2010, **147**, 531–538.
23 L. Gao, Q. H. Zhang and J. G. Li, *J. Mater. Chem.*, 2003, **13**, 154–158.
24 L. W. Yin, Y. Bando, D. Golberg and M. S. Li, *Adv. Mater.*, 2004, **16**, 1833–1838.
25 S. D. Luo, W. Y. Zhou, Z. X. Zhang, X. Y. Dou, L. F. Liu, X. W. Zhao, D. F. Liu, L. Song, Y. J. Xiang, J. J. Zhou and S. S. Xie, *Chem. Phys. Lett.*, 2005, **411**, 361–365.
26 R. C. Weast, *CRC Handbook of Chemistry and Physics*, Academic, Florida, 1983–1984.
27 Y. D. Yin, R. M. Rioux, C. K. Erdonmez, S. Hughes, G. A. Somorjai and A. P. Alivisatos, *Science*, 2004, **304**, 711–714.
28 J. Liu, W. J. Wang, Z. P. Guo, R. Zeng, S. X. Dou and X. L. Chen, *Chem. Commun.*, 2010, **46**, 3887–3889.
29 H. J. Fan, M. Knez, R. Scholz, K. Nielsch, E. Pippel, D. Hesse, M. Zacharias and U. Gösele, *Nat. Mater.*, 2006, **5**, 627.
30 H. J. Fan, M. Knez, R. Scholz, D. Hesse, K. Nielsch, M. Zacharias and U. Gösele, *Nano Lett.*, 2007, **7**, 993–997.
31 E. S. Toberer, T. D. Schladt and R. Seshadri, *J. Am. Chem. Soc.*, 2006, **128**, 1462–1463.
32 C. X. Wang, L. W. Yin, L. Y. Zhang, Y. X. Qi, N. Lun and N. N. Liu, *Langmuir*, 2010, **26**, 12841–12848.
33 K. B. Zhang, L. L. Gu, D. L. Sun, X. L. Mo and G. R. Chen, *Mater. Sci. Eng., B*, 2010, **166**, 104–107.
34 (*a*) B. R. Mehta and V. N. Singh, *Pramana–J. Phys.*, 2005, **65**, 949–958; (*b*) A. Gurlo, *Nanoscale*, 2011, **3**, 154–165.
35 C. Xu, J. Tamaki, N. Miura and N. Yamazoe, *Sens. Actuators, B*, 1991, **3**, 147–155.
36 A. Rothschild and Y. Komem, *J. Appl. Phys.*, 2004, **95**, 6374–6380.
37 L. Madler, T. Sahm, A. Gurlo, J. D. Grunwaldt, N. Barsan, U. Weimar and S. E. Pratsinis, *J. Nanopart. Res.*, 2006, **8**, 783–796.
38 A. Gurlo, N. Barsan, M. Ivanovskaya, U. Weimar and W. Gopel, *Sens. Actuators, B*, 1998, **47**, 92–99.
39 M. E. Franke, T. J. Koplin and U. Simon, *Small*, 2006, **2**, 36–50.
40 H. R. Kim, K. I. Choi, K. M. Kim, I. D. Kim, G. Z. Cao and J. H. Lee, *Chem. Commun.*, 2010, **46**, 5061–5063.

Downloaded by University of Wollongong on 03 April 2012
Published on 28 June 2011 on http://pubs.rsc.org | doi:10.1039/C1JM10537J